OPEN ACCESS Freely available online

PLOS ONE

Double Diffusive Magnetohydrodynamic (MHD) Mixed Convective Slip Flow along a Radiating Moving Vertical Flat Plate with Convective Boundary Condition

Mohammad M. Rashidi[1,2]*, Neda Kavyani[3], Shirley Abelman[4]*, Mohammed J. Uddin[5], Navid Freidoonimehr[6]

1 Mechanical Engineering Department, Engineering Faculty of Bu-Ali Sina University, Hamedan, Iran, **2** University of Michigan-Shanghai Jiao Tong University Joint Institute, Shanghai Jiao Tong University, Shanghai, People's Republic of China, **3** Sama Technical and Vocational Training College, Islamic Azad University, Malayer Branch, Malayer, Iran, **4** Centre for Differential Equations, Continuum Mechanics and Applications, School of Computational and Applied Mathematics, University of the Witwatersrand, Johannesburg, South Africa, **5** Department of Mathematics, American International University-Bangladesh, Banani, Dhaka, Bangladesh, **6** Young Researchers & Elite Club, Hamedan Branch, Islamic Azad University, Hamedan, Iran

Abstract

In this study combined heat and mass transfer by mixed convective flow along a moving vertical flat plate with hydrodynamic slip and thermal convective boundary condition is investigated. Using similarity variables, the governing nonlinear partial differential equations are converted into a system of coupled nonlinear ordinary differential equations. The transformed equations are then solved using a semi-numerical/analytical method called the differential transform method and results are compared with numerical results. Close agreement is found between the present method and the numerical method. Effects of the controlling parameters, including convective heat transfer, magnetic field, buoyancy ratio, hydrodynamic slip, mixed convective, Prandtl number and Schmidt number are investigated on the dimensionless velocity, temperature and concentration profiles. In addition effects of different parameters on the skin friction factor, $C_{f\bar{x}}$, local Nusselt number, $Nu_{\bar{x}}$, and local Sherwood number $Sh_{\bar{x}}$ are shown and explained through tables.

Citation: Rashidi MM, Kavyani N, Abelman S, Uddin MJ, Freidoonimehr N (2014) Double Diffusive Magnetohydrodynamic (MHD) Mixed Convective Slip Flow along a Radiating Moving Vertical Flat Plate with Convective Boundary Condition. PLoS ONE 9(10): e109404. doi:10.1371/journal.pone.0109404

Editor: Zhonghao Rao, China University of Mining and Technology, China

Received April 14, 2014; **Accepted** September 8, 2014; **Published** October 24, 2014

Data Availability: The authors confirm that all data underlying the findings are fully available without restriction. All relevant data are within the paper.

Funding: The authors have no support or funding to report.

Competing Interests: The authors have declared that no competing interests exist.

* Email: mm_rashidi@yahoo.com (MMR); Shirley.Abelman@wits.ac.za (SA)

Introduction

Nonlinear equations play an important role in applied mathematics, physics and issues related to engineering due to their role in describing many real world phenomena. The importance of obtaining exact or approximate solutions of nonlinear partial differential equations is still a big problem that compels scientists and engineers to seek different methods for exact or approximate solutions. A variety of numerical and analytical methods have been developed to obtain accurate approximate and analytic solutions for problems. Numerical methods give discontinuous points of a curve and thus it is very time consuming to obtain a complete curve of results. There are also some analytic techniques for nonlinear equations. Some of these analytic methods are Lyapunov's artificial small parameter method [1], δ-expansion method [2], perturbation techniques [3,4], variational iteration method (VIM) [5,6] and homotopy analysis method (HAM) [7,8].

In recent years semi-numerical/analytical methods have become popular in magnetofluid dynamics research as they provide an alternative to purely numerical methods and require significantly less computational resources. One such method, the differential transform method (DTM) was first introduced by Zhou [9] in electrical circuit theory for solving both linear and nonlinear initial value problems. Developing this method for partial differential equations and obtaining closed form series solutions for linear and nonlinear initial value problems was carried out by Chen and Ho [10] in 1999, and Ayaz [11] applied DTM to the system of differential equations.

The significant advantage of the differential transform method over numerical methods is that it does not require linearization or discretization to be applied to nonlinear differential equations and therefore is not affected by the related errors. Also, DTM does not require a perturbation parameter and also the validity is independent of whether or not there exist small parameters in the considered equation. This method has been adapted in recent years and successfully applied to simulate many multi-physical transport phenomena problems including magnetic liquid film flows [12], mixed convection flow [13], micropolar convection [14].

Magnetohydrodynamics (MHD) is concerned with the mutual interaction of fluid flow and magnetic fields. The fluids being investigated must be electrically conducting and non-magnetic, which limits the fluids to liquid metals, hot ionized gases (plasmas) and strong electrolytes. The use of an external magnetic field is a very important issue in many industrial applications, especially as a mechanism to control material construction. Some important examples of magnetohydrodynamic flow of an electrically

conducting fluid past a heated surface are MHD power generators, plasma studies, petroleum industries, cooling of nuclear reactors, the boundary- layer control in aerodynamics, and crystal growth [15,16]. The goal of the thermal treatment is to cool the material to a desirable temperature before spooling or removing it. As the high temperature material emerges from a furnace or a die, is exposed to the colder ambient, therefore transient conduction process accompanied by surface heat loss is initiated [17]. When high temperatures are encountered in the application areas, the thermal radiation effect becomes very important. High temperature plasmas, cooling of nuclear reactors, liquid metal fluids, and power generation systems are some important applications of radiative heat transfer from a surface plate to conductive fluids. There have been some studies that consider hydromagnetic radiative heat transfer flows. Spreiter and Rizzi [18] studied solar wind radiative magnetohydrodynamics. Nath et al. [19] obtained a set of similarity solutions for radiative-MHD stellar point explosion dynamics using shooting methods. Noor et al. [20] considered MHD free convection thermophoretic flow over a radiate isothermal inclined plate with heat source/sink effect.

Mixed convection flow and heat transfer over a continuously moving surface is applicable to many industrial fields such as hot rolling, paper production, wire drawing, glass fiber production, aerodynamic extrusion of plastic sheets, the boundary-layer along a liquid film, condensation process of metallic plate in a cooling bath and glass, and also in polymer industries [21]. The flow over a continuous material moving through a quiescent fluid is induced by the movement of the solid material and also by thermal buoyancy which will determine the momentum and thermal transport processes [22]. The first study of the flow field due to a surface moving with a constant velocity in a quiescent fluid was undertaken by Sakiadis [23]. Since then, other researchers investigated various aspects of mixed convection problems such as heat and (or) mass transfer, suction/injection, thermal radiation, MHD flow, porous media, slip flows, etc. [24,25].

In some situations such as the spreading of a liquid on a solid substrate, corner flow and the extrusion of polymer melts from a capillary tube, no slip conditions yield unrealistic behavior and must be replaced by slip conditions especially in applications of microfluidics and nanofluidics [26–28]. The difference between the fluid velocity at the wall and the velocity of the wall itself is directly proportional to the shear stress. The proportional factor is called the slip length. The corresponding slip boundary condition is $|u|_{\text{wall}} = l_s \left|\frac{\partial u}{\partial y}\right|$, where l_s is the slip length [29]. For gaseous flow the slip condition of the velocity and the jump condition of the temperature are $|u|_{\text{wall}} = \lambda \frac{2-\sigma_v}{\sigma_v}\left|\frac{\partial u}{\partial y}\right| + \frac{3\mu}{4\rho\, T_{gas}}\left|\frac{\partial T}{\partial x}\right|$ and $T_{\text{wall}} = \frac{2-\sigma_T}{\sigma_T}\frac{2k}{k+1}\frac{\lambda}{\text{Pr}}\frac{\partial T}{\partial y}$, respectively where σ_v and σ_T are the tangential momentum coefficient and the temperature accommodation coefficient [30]. Some relevant papers on slip flows are Kim et al. [31], Martin and Boyd [32], Kuznetsov and Nield [33].

The above researchers restricted to either prescribed temperatures or heat flux at the wall or slip. The idea of using convective boundary conditions which are the generalization of isothermal and thermal slip boundary conditions was introduced by Aziz [34] and was followed by Magyari [35] who found an exact solution of Aziz's [34] problem in a compact integral form and Ishak [36] who extended the same problem for a permeable flat plate.

The goal of the present study is to develop similarity transformations via one parameter linear group of transformations and the corresponding similarity solutions for mixed convection flow of viscous incompressible fluid past a moving vertical flat plate with thermal convective and hydrodynamic slip boundary conditions and to solve the transformed coupled ordinary differential equations using the differential transform method. The effects of the Prandtl numberPr, the Schmidt number Sc, the mixed convective parameter Ri, the buoyancy ratio parameter N, the radiation parameter R, the magnetic field parameter M and the slip parameter a on the flow, heat and mass transfer characteristics are investigated numerically.

In section 2 the geometry of the flow along a moving vertical flat plate under consideration in this problem is modeled with hydrodynamic slip and thermal convective boundary condition assumptions. The system with two independent variables is reduced to one variable equations and a system of nonlinear ordinary differential equations is obtained using a linear group of transformations. Sections 3 and 4 provide methods of solution for the governing equations of the problem, the differential transform method and numerical solution, respectively. In section 5 physical reasons are illustrated for the behavior of the graphs and tables of the problem, and finally inferences are made and conclusions are drawn.

Nomenclature

B magnetic field strength
C concentration
C_w wall concentration
C_∞ ambient concentration
D diffusion coefficient (m^2/s)
$f(\eta)$ dimensionless stream function
g acceleration due to gravity (m/s^2)
h_s heat transfer coefficient ($W/m^{2\cdot}K$)
k thermal conductivity (W/m.K)
L characteristic length (m)
N buoyancy ratio parameter
$Nu_{\bar{x}}$ local Nusselt number
Pr Prandtl number
p pressure (N/m^2)
q_m wall mass flux ($kg/s\ m^2$)
q_w wall heat flux (W/m^2)
Ri mixed convective parameter
$Gr_{\bar{x}}$ local Grashof number
$Sh_{\bar{x}}$ local Sherwood number
T temperature inside boundary layer (K)
T_w wall temperature (K)
T_∞ ambient temperature (K)
$\bar{u}, \bar{v}$ velocity components along $\bar{x}-$ and $\bar{y}-$axes (m/s)
$\bar{x}, \bar{y}$ Cartesian coordinates along and normal to the plate (m)

Greek Symbols

α thermal diffusivity of the porous medium (m^2/s)
β_T volumetric thermal expansion coefficient of the base (1/K)
β_C volumetric solutal expansion coefficient of the base (1/K)
μ absolute viscosity of the base fluid (Ns/m^2)
υ kinematic viscosity of the fluid (m^2/s)
σ electric conductivity
γ convective heat transfer parameter
$\phi(\eta)$ dimensionless concentration function
η similarity variable
$\theta(\eta)$ dimensionless temperature
ρ fluid density (kg/m^3)
ψ stream function

Mathematical Modeling

Figure 1 shows the geometry assumed in this study, along with the rectangular coordinates, $\bar{x}$ and $\bar{y}$, and the corresponding velocity components, $\bar{u}$ and $\bar{v}$ (where i represents momentum, ii represents thermal and concentration boundary-layers and in general thermal and concentration boundary-layer thickness are not the same). The temperature of the ambient fluid is T_∞, the unknown temperature of the plate is T_w and the left surface of the plate is heated from a hot fluid of temperature T_f ($>T_\infty$) or is cooled from a cooled fluid ($T_f<T_\infty$) by the process of convection which yields a heat transfer variable coefficient $h_f(\bar{x})$. It is also assumed that the ambient fluid is of uniform concentration C_∞, the unknown concentration of the plate is C_w. A transverse magnetic field with variable strength $B(\bar{x})=B_0/\bar{x}^{1/2}$ is applied parallel to the $\bar{y}$ axis, where B_0 is the constant magnetic field [37]. Variable electric conductivity $\sigma=\sigma_0\,\bar{u}$ is assumed, where σ_0 is the constant electric conductivity [37]. The magnetic Reynolds number is assumed to be small and hence the induced magnetic field can be neglected. Fluid properties are invariant except density, which is assumed to vary only in those changes that drive the flow (i.e., the Boussinesq approximation). Under the assumption of boundary-layer approximations, the governing boundary-layer equations in dimensional form are:

$$\frac{\partial\,\bar{u}}{\partial\bar{x}}+\frac{\partial\bar{v}}{\partial\bar{y}}=0, \tag{1}$$

$$\begin{aligned}&\rho\left(\bar{u}\frac{\partial\bar{u}}{\partial\bar{x}}+\bar{v}\frac{\partial\bar{u}}{\partial\bar{y}}\right)=\\&\mu\frac{\partial^2\bar{u}}{\partial\bar{y}^2}+[\rho g\beta_T\,(T-T_\infty)+\rho g\beta_C\,(C-C_\infty)]-\frac{\sigma_0B_0^2}{\bar{x}}\,\bar{u}^2,\end{aligned} \tag{2}$$

$$\bar{u}\frac{\partial T}{\partial\bar{x}}+\bar{v}\frac{\partial T}{\partial\bar{y}}=\left(\alpha+\frac{16\,\sigma_1T_\infty^3}{3\,\rho\,c_p\,k_1}\right)\frac{\partial^2T}{\partial\bar{y}^2}, \tag{3}$$

$$\bar{u}\frac{\partial C}{\partial\bar{x}}+\bar{v}\frac{\partial C}{\partial\bar{y}}=D\frac{\partial^2C}{\partial\bar{y}^2}, \tag{4}$$

subject to the boundary conditions:

$$\begin{aligned}&\bar{v}=0,\bar{u}=U_w+U_{\text{slip}}\\&=U_r\left(\frac{x}{L}\right)^{1/2}+N_1\upsilon\,\frac{\partial\,\bar{u}}{\partial\,\bar{y}},-k\,\frac{\partial\,T}{\partial\,\bar{y}}\\&=h_f(\bar{x})\,\left[T_f-T_w\right],\ C=C_w\ \text{ at }\ \bar{y}=0,\end{aligned} \tag{5}$$

$$\bar{u}\to0,\quad T\to T_\infty,\quad C\to C_\infty\quad\text{as}\quad\bar{y}\to\infty,$$

where T is the temperature, C is the concentration, υ is the kinematic viscosity, k is the thermal conductivity, α is the thermal diffusivity, D is the mass diffusivity of species of the fluid, β_T is the volumetric thermal coefficient, β_C is the volumetric concentration coefficient, g is the acceleration due to gravity, σ_1 is the Stefan-Boltzmann constant, k_1 is the Rosseland mean absorption coefficient, $\alpha=k/\rho\,c_p$ is the thermal diffusivity of the fluid, ρ is the density of the fluid, μ is viscosity, $h_f(\bar{x})$ is the heat transfer coefficient and N_1 is the velocity slip factor.

2.1 Normalization

The following boundary-layer variables are introduced to express Eqs. (1)–(5) in dimensionless form:

$$\begin{aligned}&x=\frac{\bar{x}}{L},y=\frac{\bar{y}\,\mathrm{Re}^{1/2}}{L},\\&u=\frac{\bar{u}}{U_0},v=\frac{\bar{v}\,L}{\upsilon\,\mathrm{Re}^{1/2}},\ \theta=\frac{T-T_\infty}{T_f-T_\infty},\ \phi=\frac{C-C_\infty}{C_w-C_\infty},\end{aligned} \tag{6}$$

where $\mathrm{Re}=U_0L/\upsilon$ is the Reynolds number based on the characteristic length L and characteristic velocity U_0. The stream function ψ defined as $u=\frac{\partial\psi}{\partial y},v=-\frac{\partial\psi}{\partial x}$ is substituted into Eqs. (2)–(5) to reduce the number of equations and number of dependent variables. Therefore the following three dimensionless equations are obtained:

$$\frac{\partial\psi}{\partial y}\frac{\partial^2\psi}{\partial x\,\partial y}-\frac{\partial\psi}{\partial x}\frac{\partial^2\psi}{\partial y^2}-\frac{\partial^3\,\psi}{\partial y^3}-Ri\,[\theta+N\,\phi]+\frac{M}{x}\left(\frac{\partial\psi}{\partial y}\right)^2=0, \tag{7}$$

$$\mathrm{Pr}\left(\frac{\partial\psi}{\partial y}\frac{\partial\theta}{\partial x}-\frac{\partial\psi}{\partial x}\frac{\partial\theta}{\partial y}\right)-(1+R)\frac{\partial^2\theta}{\partial y^2}=0, \tag{8}$$

$$Sc\left(\frac{\partial\psi}{\partial y}\frac{\partial\phi}{\partial x}-\frac{\partial\psi}{\partial x}\frac{\partial\phi}{\partial y}\right)-\frac{\partial^2\,\phi}{\partial\,y^2}=0. \tag{9}$$

Here $\mathrm{Pr}=\upsilon/\alpha$ is the Prandtl number, $Sc=\upsilon/D$ is the Schmidt number, $N=\beta_C(C_w-C_\infty)/\beta_T(T_f-T_\infty)$ is the buoyancy ratio parameter, $M=\sigma_0\,B_0^2/\rho$ is the magnetic field parameter, $R=16\,\sigma_1\,T_\infty^3/3\,k_1k$ is the radiation parameter, $Gr=g\beta_T\left(T_f-T_\infty\right)L^3/\upsilon^2$ is the Grashof number, $Ri=Gr/\mathrm{Re}^2$ is the mixed convective parameter [38], $Ri>0$ is for aiding buoyancy flow and $Ri<0$ is for opposing buoyancy flow and $Ri=0$ is for purely forced convective flow in which buoyancy effects are not present.

The boundary conditions take the following form:

$$\begin{aligned}&\frac{\partial\,\psi}{\partial y}=x^{1/2}+\frac{\mathrm{Re}^{1/2}N_1(x)\,\upsilon}{L}\,\frac{\partial^2\,\psi}{\partial y^2},\ \frac{\partial\psi}{\partial x}=0,\\&\frac{\partial\theta}{\partial y}=-\frac{L\,h_f(x)}{k\,\mathrm{Re}^{1/2}}(1-\theta),\ \ \phi=1\ \text{at}\ y=0\,,\end{aligned} \tag{10}$$

$$\frac{\partial\,\psi}{\partial y}\to0,\ \theta\to0,\ \phi\to0\quad\text{as}\quad y\to\infty.$$

2.2 Application of Linear Group Analysis and Similarity Equations

The transport Eqs. (7)–(10) form a highly coupled nonlinear boundary value problem. Numerical solutions of these equations are complicated and time consuming. In this section the linear

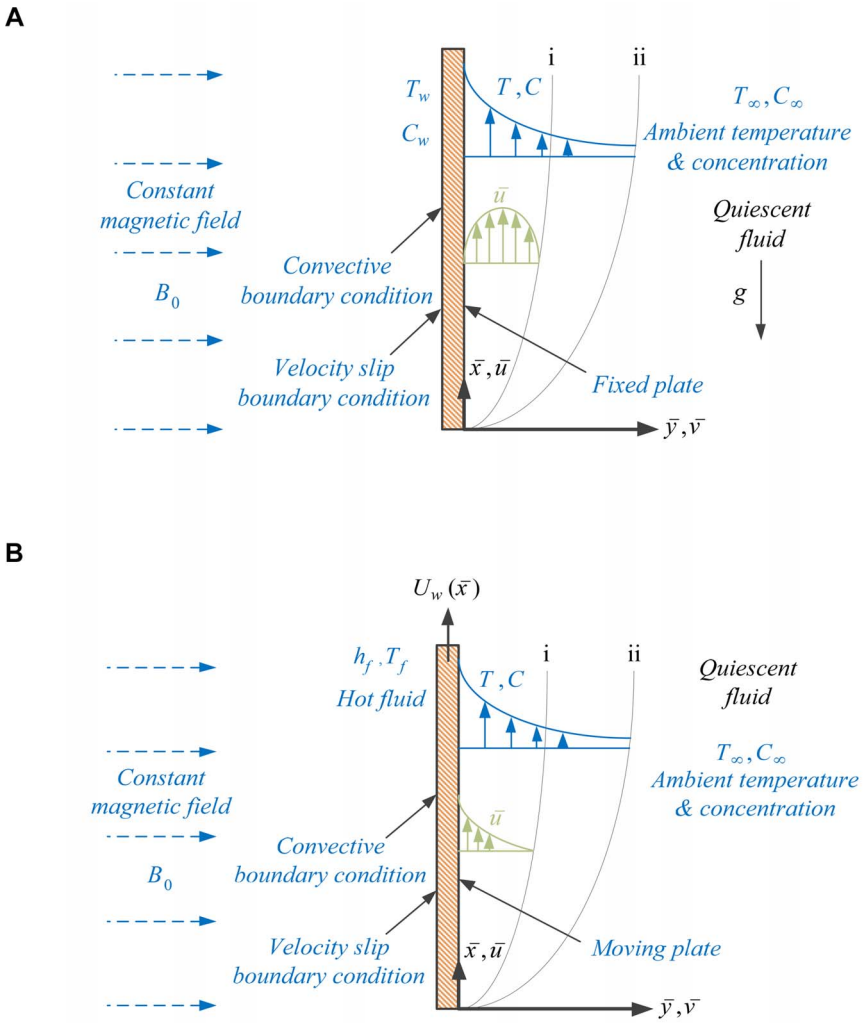

Figure 1. Flow configuration and coordinate system for an assisting flow (a) fixed plate, (b) moving plate.
doi:10.1371/journal.pone.0109404.g001

group of transformations is imposed on the problem to combine the two independent variables (x,y) into a single independent variable η (similarity variable) and reduce Eqs. (7)–(10) into ordinary differential equations with corresponding boundary conditions. For this purpose all independent and dependent variables are scaled as:

$$\begin{aligned} &x^* = x A^{\alpha_1},\ y^* = y A^{\alpha_2},\ \psi^* = \psi A^{\alpha_3}, \\ &\theta^* = \theta A^{\alpha_4}, \phi^* = \phi A^{\alpha_5}, h_f{}^* = h_f A^{\alpha_6}, N_1{}^* = N_1 A^{\alpha_7}, \end{aligned} \tag{11}$$

where A, $\alpha_i\,(i=1,2,\ldots,6,7)$ are constants, the values of α_i should be chosen such that the form of the Eqs. (7)–(10) is invariant under the transformations. Eqs. (7)–(10) will be invariant if α_i are related by

$$\alpha_1 = 4\alpha_2,\ \alpha_3 = 3\alpha_2,\ \alpha_4 = \alpha_5 = 0, \alpha_6 = -\alpha_2,\ \alpha_7 = \alpha_2. \tag{12}$$

It is clear from Eqs. (11) and (12) that

$$\frac{y}{x^{1/4}} = \frac{y^*}{x^{*1/4}}. \tag{13}$$

This combination of variables is invariant under this group of transformations and consequently, is an absolute invariant which are functions having the same form before and after the transformation. This functional form is denoted using

$$\eta = \frac{y}{\sqrt[4]{x}}, \tag{14}$$

where η is the similarity independent variable. By the same argument, other absolute invariants are

$$\begin{aligned} &\psi = x^{3/4} f(\eta), \theta = \theta(\eta),\ \phi = \phi(\eta), \\ &h_f = x^{-1/4} (h_f)_0, N_1 = x^{1/4} (N_1)_0, \end{aligned} \tag{15}$$

where $f(\eta)$, $\theta(\eta)$ and $\phi(\eta)$ are the dimensionless velocity, temperature, concentration function, $(h_f)_0$ is the constant heat transfer coefficient, $(N_1)_0$ is the constant hydrodynamic slip factor.

Substituting Eqs. (14) and (15) into Eqs. (7)–(9), the following ordinary differential equations are obtained

$$f''' + \frac{1}{4}\left(3ff'' - 2f'^2 - 4Mf'^2\right) + Ri\,\theta + Ri\;N\,\phi = 0, \quad (16)$$

$$(1+R)\theta'' + \frac{3\,\mathrm{Pr}}{4} f\;\theta' = 0, \quad (17)$$

$$\phi'' + \frac{3\,Sc}{4} f\,\phi' = 0, \quad (18)$$

subject to the boundary conditions

$$\begin{aligned} &f(0)=0, f'(0)=1+af''(0),\\ &\theta'(0) = -Bi\,[1-\theta(0)]\;, \phi(0)=1,\, f'(\infty) = \theta(\infty)=\phi(\infty)=0, \end{aligned} \quad (19)$$

where primes denote differentiation with respect to η. Here $Bi = (h_f)_0\, L/k\, Ra^{1/2}$ is the Biot number and $a = (N_1)_0 \upsilon\, \mathrm{Re}^{1/2}/L$ is the hydrodynamic slip parameter. Nondimensionalizing procedure is explained in detail in **Appendix A**.

2.3 Quantities of Engineering Interest

The physical parameters of interest in the present problem are the skin friction factor $C_{f\bar{x}}$, local Nusselt number $Nu_{\bar{x}}$ and local Sherwood number $Sh_{\bar{x}}$ which may be determined, respectively by the following expressions:

$$\begin{aligned} &C_{f\bar{x}} = \frac{\mu}{\rho\, U_w^2(\bar{x})}\left(\frac{\partial \bar{u}}{\partial \bar{y}}\right)_{\bar{y}=0},\\ &Nu_{\bar{x}} = \frac{\bar{x}}{\Delta T}\left(-\frac{\partial T}{\partial \bar{y}}\right)_{\bar{y}=0}, \quad Sh_{\bar{x}} = \frac{\bar{x}}{\Delta C}\left(-\frac{\partial C}{\partial \bar{y}}\right)_{\bar{y}=0}. \end{aligned} \quad (20)$$

Using Eqs. (6), (14), (15), we have from Eq. (20)

$$\begin{aligned} &\mathrm{Re}_{\bar{x}}^{1/2}\, C_{f\bar{x}} = f''(0),\\ &\mathrm{Re}_{\bar{x}}^{-1/2}\; Nu_{\bar{x}} = -\,\theta'(0), \quad \mathrm{Re}_{\bar{x}}^{-1/2}\; Sh_{\bar{x}} = -\,\phi'(0), \end{aligned} \quad (21)$$

where $\mathrm{Re}_x = U\,\bar{x}/\upsilon$ is the local Reynolds number.

The Differential Transform Method

DTM is employed to obtain semi-analytical/numerical solutions to the well-posed two-point boundary value problem defined by Eqs. (16)–(18) and conditions (19). DTM is an extremely strong technique in finding solutions to magnetohydrodynamic and complex material flow problems. It has also been used very effectively in conjunction with Padé approximants. Rashidi et al. [39] studied transient magnetohydrodynamic flow, heat transfer and entropy generation from a spinning disk using DTM- Padé. To provide a summary of the method, the transformation of the k^{th} derivative of a function in one variable is considered which is defined as:

$$F(k) = \frac{1}{k!}\left[\frac{d^k f(\eta)}{d\eta^k}\right]_{\eta=\eta_0}, \quad (22)$$

where $f(\eta)$ is the original function and $F(k)$ is the transformed function. The differential inverse transform of $F(k)$ is:

$$f(\eta) = \sum_{k=0}^{\infty} F(k)(\eta-\eta_0)^k. \quad (23)$$

The concept of the differential transform is derived from a Taylor series expansion and in actual applications the function $f(\eta)$ is expressed by a finite series as follows:

$$f(\eta) = \sum_{k=0}^{m} F(k)(\eta-\eta_0)^k. \quad (24)$$

The value of m is decided by convergence of the series coefficients. The fundamental mathematical operations performed by DTM are listed in **Table 1**. Taking differential transforms of Eqs. (16)–(18), the following transformed equations are obtained:

$$\begin{aligned} &(k+1)(k+2)(k+3)F[k+3] =\\ &\left(\sum_{r=0}^{k}\begin{pmatrix}(-3/4)(k-r+1)(k-r+2)F[r]F[k-r+2]\\ +(0.5+M)(k-r+1)(r+1)F[r+1]F[k-r+1]\end{pmatrix}\right.\\ &\left. -Ri\,\Theta[k] - Ri\;N\,\Phi[k]\right), \end{aligned} \quad (25)$$

$$\begin{aligned} &(k+2)(k+1)\Theta[k+2] =\\ &(1/(1+R))\left(\sum_{r=0}^{k} -(3/4)\mathrm{Pr}(k-r+1)F[r]\Theta[k-r+1]\right), \end{aligned} \quad (26)$$

$$\begin{aligned} &(k+2)(k+1)\Phi[k+2] =\\ &\sum_{r=0}^{k}(-(3/4)Sc(k-r+1)F[r]\Phi[k-r+1]), \end{aligned} \quad (27)$$

where $F(k)$, $\Theta(k)$ and $\Phi(k)$ are the differential transform of $f(\eta)$, $\theta(\eta)$ and $\phi(\eta)$, respectively, and the transformed boundary conditions are:

$$F[0]=0, F[1]=\alpha,\; F[2]=\beta, \quad (28)$$

$$\theta\,[0]=\gamma,\; \theta\,[1]=\delta, \quad (29)$$

$$\Phi\,[0]=1,\; \Phi\,[1]=\varepsilon, \quad (30)$$

where α, β, γ, δ and ε are constants which are computed from the boundary conditions.

Here Páde approximants are applied to the problem to increase the convergence of a given series. As shown in Fig. 2, without using the Páde approximant, the different orders of the DTM

Table 1. Operations for DTM.

Transformed function	Original function
$F(k)=G(k)\pm H(k)$	$f(\eta)=g(\eta)\pm h(\eta)$
$F(k)=\lambda\, G(k)$, λ is a constant	$f(\eta)=\lambda\, g(\eta)$
$F(k)=(k+1)(k+2)$ ...$(k+r)G(k+r)$	$f(\eta)=\frac{d^r g(\eta)}{d\eta^r}$
$F(k)=\sum_{r=0}^{k} G(r)H(k-r)$	$f(\eta)=g(\eta)\,h(\eta)$
$F(k)=\sum_{r=0}^{k}(k-r+1)\,G(r)H(k-r+1)$	$f(\eta)=g(\eta)\frac{dh(\eta)}{d\eta}$
$F(k)=\sum_{r=0}^{k}(k-r+1)(k-r+2)G(r)H(k-r+2)$	$f(\eta)=g(\eta)\frac{d^2h(\eta)}{d\eta^2}$

doi:10.1371/journal.pone.0109404.t001

solution, cannot satisfy the boundary conditions at infinity. Therefore, it is necessary to use DTM-Páde to provide an effective way to handle boundary value problems with boundary conditions at infinity. See **Appendix B** for a description of the Páde approximant method.

Numerical Solution

The system of nonlinear differential equations (16)–(18) is solved under the boundary conditions (19). The initial boundary conditions for f and θ in (19) are unknown in comparison with the case of no-slip and no jump condition of the temperature boundary conditions. Hence, the solution of the system cannot

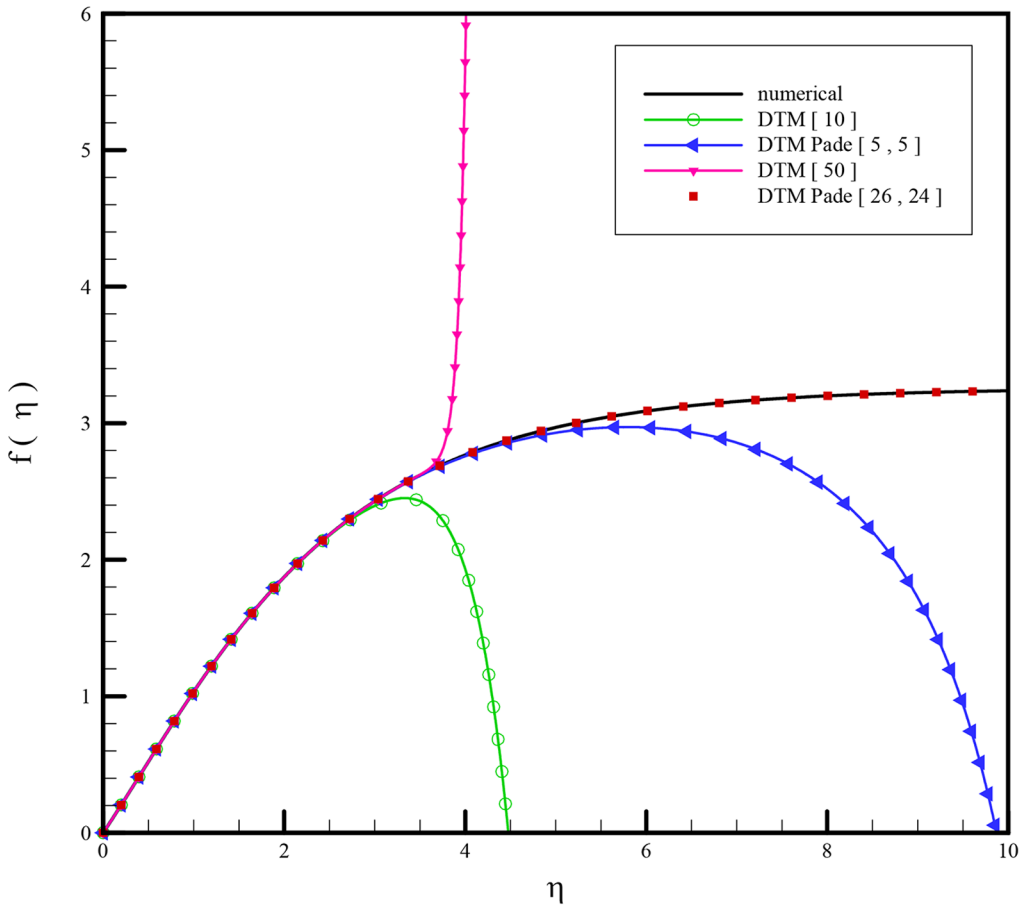

Figure 2. The analytical solution of $f(\eta)$ obtained by DTM, DTM-Padé and numerical method for $a=1$, $\mathrm{Pr}=0.72$, $Sc=0.2$, $Ri=1$, $M=0.2$ and $N=1$.
doi:10.1371/journal.pone.0109404.g002

proceed numerically using any standard integration routine. Here, following [40–41], a second order numerical technique is adopted. This technique combines the features of the finite difference method and the shooting method and is accurate because it uses central differences.

The semi-infinite integration domain $\eta \in [0,\infty)$ is replaced by a finite domain $\eta \in [0,\eta_\infty)$ and η_∞ should be chosen sufficiently large so that the numerical solution closely approximates the terminal boundary conditions (19). Here a large enough finite value has been substituted for η_∞, the numerical infinity, to ensure that the solutions are not affected by imposing the asymptotic conditions at a finite distance. The value of η_∞ has been kept invariant during the run of the program.

Now a mesh is defined by $\eta_i = ih$ $(i=0,1,...,n)$, with h being the mesh size, and Eqs. (16)–(18) are discretized using central difference approximations for the derivatives, the following equations are obtained at the i^{th} mesh point:

$$\frac{F_{i+2}-2F_{i+1}+2F_{i-1}-F_{i-2}}{2h^3}+\frac{1}{4}(3F_i\left(\frac{F_{i+1}-2F_i+F_{i-1}}{h^2}\right)- 2\left(\frac{F_{i+1}-F_{i-1}}{2h}\right)^2-4M\left(\frac{F_{i+1}-F_{i-1}}{2h}\right)^2)+Ri\,\theta_i+Ri\,N\,\phi_i=0, \quad (31)$$

$$(1+R)\frac{\theta_{i+1}-2\theta_i+\theta_{i-1}}{h^2}+\frac{3\,\mathrm{Pr}}{4}\,F_i\left(\frac{\theta_{i+1}-\theta_{i-1}}{2h}\right)=0, \quad (32)$$

$$\frac{\phi_{i+1}-2\phi_i+\phi_{i-1}}{h^2}+\frac{3\,Sc}{4}\,F_i\left(\frac{\phi_{i+1}-\phi_{i-1}}{2h}\right)=0. \quad (33)$$

Note that Eqs. (16)–(18), which are written at the i^{th} mesh point, the first, second and third derivatives are approximated by central differences centered at i^{th} mesh point. This scheme ensures that the accuracy of $O(h^2)$ is preserved in the discretization.

Eqs. (31)–(33) are term recurrence relations in F, θ and ϕ. So, in order to start the recursion, besides the values of F_0, θ_0 and ϕ_0, the values of F_1, F_2, θ_1 and ϕ_1 are also required. These values can be obtained by Taylor series expansion near $\eta=0$ for F, θ and ϕ, with initial assumptions for the dimensionless functions of F and θ.

The values of $F(0)$, $F'(0)$, $\theta(0)$ and $\phi(0)$ are given as boundary conditions in (19). The values of $F'''(0)$, $\theta''(0)$ and $\phi''(0)$ can be obtained directly from Eqs. (10)–(12) and using the initial assumptions. After obtaining the values of F_1, θ_1 and ϕ_1, at the next cycle F_2, θ_2 and ϕ_2 are obtained. The order indicated above is followed for the subsequent cycles. The integration is carried out until the values of F, θ and ϕ are obtained at all the mesh points.

The three asymptotic boundary conditions (13) and (14) must be satisfied. Initial assumptions are found by applying a shooting method along with the fourth order Runge–Kutta method so as to fulfill the free boundary conditions at $\eta=\eta_\infty$ in (19). The guesses can be improved by a suitable zero-finding algorithm, including Newton's method, Broyden's, etc. [42,43].

Results and Discussion

A linear group of transformations is used to reduce the two independent variables into one and reduce the governing equations into a system of nonlinear ordinary differential equations with associated boundary conditions. Equations (16)–(18) with boundary conditions (19) were solved analytically using the differential transform method and compared with numerical results. Figure 2 shows the results of comparison and great agreement is seen. Typically, the natural convection is negligible when $Ri<0.1$, forced convection is negligible when $Ri>10$, and neither is negligible when $0.1< Ri<10$. It is useful to note that usually the forced convection is large relative to natural convection except in the case of extremely low forced flow velocities. Here $Ri > 0$ is chosen to have aiding buoyancy flow.

For Biot number smaller than 0.1 the heat conduction inside the body is quicker than the heat convection away from its surface, and temperature gradients are negligible inside of it. Having a Biot number smaller than 0.1 labels a substance as thermally thin, and temperature can be assumed to be constant throughout the materials volume. The opposite is also true: A Biot number greater than 0.1 (a "thermally thick" substance) indicates that one cannot make this assumption, and more complicated heat transfer equations for "transient heat conduction" will be required to describe the time-varying and non-spatially-uniform temperature field within the material body. In this research the case of cooling of the plate $Gr > 0$ is assumed and also the value of 0.5 is chosen for the Biot number and the thermal radiation number is equal to 1 in all diagrams as the control parameters.

In **Tables 2–6** effects of some of the parameters on the Skin friction factor, $C_{f\bar{x}}$, local Nusselt number, $Nu_{\bar{x}}$, and local Sherwood number, $Sh_{\bar{x}}$ are shown. According to **Table 2**, increasing the buoyancy ratio parameter, N, causes $\mathrm{Re}_{\bar{x}}^{1/2}\,C_{f\bar{x}}$, $\mathrm{Re}_{\bar{x}}^{-1/2}\,Nu_{\bar{x}}$ and $\mathrm{Re}_{\bar{x}}^{-1/2}\,Sh_{\bar{x}}$ to increase. $N=\beta_C(C_w-C_\infty)/\beta_T(T_f-T_\infty)$ represents the relative magnitude of species buoyancy and thermal buoyancy forces. For $N=1$ these two forces are of the same magnitude. For $N>0$, the species buoyancy force is dominant and vice versa for $N<1$. The weaker contribution of the thermal buoyancy force for $N<1$ results in a depletion in the local Nusselt number. The stronger contribution of the species buoyancy force for $N>1$ induces enhancement in the local Sherwood number. The momentum field is coupled to the concentration (species) field via the linear species buoyancy force, $Ri\,N\,\phi$, in the momentum Eq. (16). The species field is coupled to the momentum field via the nonlinear term, $3Scf\phi'/4$, in the species diffusion Eq. (18). Both terms are assistive. The influence of N on both species diffusion and momentum diffusion is therefore very strong as observed in the very large magnitudes of skin friction and local Sherwood number in Table 2.

In **Table 3**, increasing the mixed convective parameter is observed to strongly increase skin friction and accelerate the boundary-layer flow. Only $Ri>0$ is considered corresponding to *buoyancy-assisted* flow. In the range $0.1 < Ri < 10$ both free (natural) and forced convection modes contribute. For $Ri>10$, forced convection effects are negated and for $Ri < 0.1$ free convection effects vanish. Evidently at low Ri values, buoyancy has a lesser influence on the flow characteristics and skin friction is found to be negative (flow reversal). With Ri exceeding unity any flow reversal is eliminated and the flow is strongly accelerated. Stronger buoyancy effects therefore act to stabilize the flow and aid momentum development. This simultaneously encourages more efficient diffusion of heat and species resulting in a marked increase in heat and mass transfer rates ($\mathrm{Re}_{\bar{x}}^{1/2}\,C_{f\bar{x}}$, $\mathrm{Re}_{\bar{x}}^{-1/2}\,Nu_{\bar{x}}$) at the plate.

In **Table 4** increasing the value of hydrodynamic slip parameter, a, decreases $\mathrm{Re}_{\bar{x}}^{1/2}\,C_{f\bar{x}}$but weakly increases $\mathrm{Re}_{\bar{x}}^{-1/2}\,Nu_{\bar{x}}$ and $\mathrm{Re}_{\bar{x}}^{-1/2}\,Sh_{\bar{x}}$. Momentum slip is simulated in the wall velocity boundary condition given in Eq. (19). Increasing momentum slip causes a reduction in the penetration of the

Table 2. The Skin friction factor, $C_{f\bar{x}}$, local Nusselt number, $Nu_{\bar{x}}$ and local Sherwood number, $Sh_{\bar{x}}$ for different values of the buoyancy ratio parameter N, at $\Pr = 0.72$, $M = 0.2$, $Sc = 0.2$, $Ri = 1$, $Bi = 0.5$, $R = 1$ and $a = 1$.

N	$\mathrm{Re}_{\bar{x}}^{1/2} C_{f\bar{x}}$	$\mathrm{Re}_{\bar{x}}^{-1/2} Nu_{\bar{x}}$	$\mathrm{Re}_{\bar{x}}^{-1/2} Sh_{\bar{x}}$
0.1	−0.123402	0.196943	0.220788
1.0	0.118811	0.221377	0.275433
5.0	0.860543	0.259651	0.378371
10.0	1.522606	0.279651	0.444757
50.0	4.644088	0.326977	0.662252
100.0	7.129046	0.346306	0.789132

doi:10.1371/journal.pone.0109404.t002

stagnant surface through the boundary-layer. This serves to enhance momentum boundary-layer thickness since the flow is decelerated with increasing slip so that skin friction is lowered.

Bi arises in the wall temperature gradient boundary condition in Eq. (19). As *Bi* increases from < 0.1 (thermally thin case) to > 0.1 (thermally thick case) the rate of thermal conduction heat transfer inside the plate becomes dramatically lower than the heat convection away from its surface, and temperature gradients are increased at the plate. The influence on the flow is to accelerate it. Skin friction is elevated and therefore momentum boundary-layer thickness decreased. As shown in **Table 5**, an increase in the value of Biot number, *Bi*, increases $\mathrm{Re}_{\bar{x}}^{1/2} C_{f\bar{x}}$, $\mathrm{Re}_{\bar{x}}^{-1/2} Nu_{\bar{x}}$ and $\mathrm{Re}_{\bar{x}}^{-1/2} Sh_{\bar{x}}$.

Table 6 demonstrates that an increase in Schmidt number, *Sc*, decreases both $\mathrm{Re}_{\bar{x}}^{1/2} C_{f\bar{x}}$ and $\mathrm{Re}_{\bar{x}}^{-1/2} Nu_{\bar{x}}$, whereas it increases $\mathrm{Re}_{\bar{x}}^{-1/2} Sh_{\bar{x}}$. Schmidt number is the ratio of viscous diffusion to molecular (species) diffusion. For $Sc < 1$, molecular diffusion rate exceeds the momentum diffusion rate and vice versa for $Sc > 1$. Sub-unity values of Schmidt number will therefore result in a deceleration in the flow (reduced skin friction), which will also decrease thermal diffusion rates. Conversely mass transfer will be accentuated in the regime with increasing *Sc* values.

In **Fig. 2** results using different orders of DTM and DTM-Páde are compared with those of the numerical method. Very good agreement is observed for DTM-Páde and the numerical method. In figures **3. a**–**3. f** effects of different parameters are investigated on the flow regime and the following results are observed:

- **Fig. 3. a** shows how the flow responds to change in the magnetic field. Increasing magnetic interaction number M from purely hydrodynamic case $M = 0$ to higher values of M, gives rise to a strong deceleration in the flow. Presence of a magnetic field in an electrically conducting fluid introduces a Lorentz force which acts against the flow in the case that magnetic field is applied in the normal direction as considered in the present problem. The described type of resistive force tends to slow down the flow field.
- A positive rise in N induces an increase in the flow along the plate as seen in **Fig. 3. b.**
- There is a clear decrease in the velocity values at the wall accompanying a rise in Prandtl number because the flow is decelerated. Fluids with higher Prandtl numbers will therefore possess higher viscosities (and lower thermal conductivities) which means that such fluids flow slower than lower Pr fluids (**Fig. 3. c**). As a result the velocity will be decreased substantially with increasing Prandtl number.
- According to **Fig. 3. d**, a strong mixed convective parameter has a significant acceleration effect on the boundary-layer flow.
- Through changing the values of Pr and *Sc*, the thermal and species diffusion regions change. As illustrated in **Fig. 3. e**, the dimensionless stream function $f(\eta)$ decreases as a result of increasing Schmidt number.
- **Fig. 3. f**, results from comparing the flow in the presence of slip and no slip boundary condition. The change in profiles for different values of a is not so much. In fact a influences the flow of the liquid past the moving plate and the amount of slip $1 - f'(0)$ increases monotonically with a from the no-slip

Table 3. The Skin friction factor, $C_{f\bar{x}}$, local Nusselt number, $Nu_{\bar{x}}$ and local Sherwood number, $Sh_{\bar{x}}$ for different values of the mixed convective parameter, Ri, with $\Pr = 0.72$, $M = 0.2$, $Sc = 0.2$, $a = 1$, $Bi = 0.5$, $R = 1$ and $N = 1$.

Ri	$\mathrm{Re}_{\bar{x}}^{1/2} C_{f\bar{x}}$	$\mathrm{Re}_{\bar{x}}^{-1/2} Nu_{\bar{x}}$	$\mathrm{Re}_{\bar{x}}^{-1/2} Sh_{\bar{x}}$
0.2	−0.274494	0.202957	0.300044
0.5	−0.083130	0.203855	0.237817
0.8	0.043656	0.215523	0.262461
1.0	0.118720	0.221333	0.275481
3.0	0.684401	0.251875	0.353565
5.0	1.101863	0.266782	0.398851
7.0	1.451164	0.276702	0.432251
9.0	1.758446	0.284122	0.459204

doi:10.1371/journal.pone.0109404.t003

Table 4. The Skin friction factor, $C_{f\bar{x}}$, local Nusselt number, $Nu_{\bar{x}}$ and local Sherwood number, $Sh_{\bar{x}}$ for different values of the hydrodynamic slip parameter, a, with $\mathrm{Pr}=0.72$, $M=0.2$, $Sc=0.2$, $Ri=1$, $Bi=0.5$, $R=1$ and $N=1$.

a	$\mathrm{Re}_{\bar{x}}^{1/2}\,C_{f\bar{x}}$	$\mathrm{Re}_{\bar{x}}^{-1/2}\,Nu_{\bar{x}}$	$\mathrm{Re}_{\bar{x}}^{-1/2}\,Sh_{\bar{x}}$
0.0	0.297625	0.218942	0.271244
0.2	0.229317	0.219876	0.272890
0.4	0.186188	0.220452	0.273911
0.6	0.156595	0.220841	0.274604
0.8	0.135608	0.221122	0.275104
1.0	0.118720	0.221333	0.275481
2.0	0.073893	0.221906	0.276507
4.0	0.042066	0.222307	0.277227
6.0	0.029397	0.222465	0.277512
8.0	0.022592	0.222550	0.277665
10.0	0.018345	0.222602	0.277760

doi:10.1371/journal.pone.0109404.t004

situation of $a=0$ and towards full slip as $a\to\infty$. In the limiting case the frictional resistance between the cooling liquid and the moving plate is eliminated, and the moving plate no longer imposes any motion of the cooling liquid.

Figures **4. a**–**4. f** show how heat transfer is influenced by different parameters:

- The magnetic field increases the temperature of the fluid inside the boundary-layer as a result of excess heating and consequently decreases in the heat flux, as shown in **Fig. 4. a**.
- A positive rise in N causes the temperature to decrease as seen in **Fig. 4. b**.
- **Fig. 4. c.** depicts the effects of the Prandtl number Pr on the temperature profiles $\theta(\eta)$. Prandtl number shows the ratio of momentum diffusivity to thermal diffusivity. The figure reveals that an increase in the Prandtl number Pr, results in a decrease in the temperature distribution at a particular point of the flow region. The lowest temperatures correspond to the highest value of Prandtl number. No temperature overshoot is observed. The increase in the Prandtl number means a slow rate of thermal diffusion. Larger Pr values imply a thinner thermal boundary-layer thickness and more uniform temperature distributions across the boundary-layer. Smaller Pr fluids have higher thermal conductivities so that heat can diffuse away from the vertical surface faster than for higher Pr fluids (thicker boundary-layers).
- According to **Fig. 4. d**, temperature decreases by increasing the value of the Richardson number.
- Temperature continuously increases with increasing Schmidt number as depicted in **Fig. 4. e**.
- In **Fig. 4. f**. changing the slip parameter a does not affect temperature profiles much.

Figures **5. a**–**5. f** show how the concentration profiles vary through changing different parameters entering into the problem.

- According to **Fig. 5. a** concentrations increase by increasing the value of M.
- Concentration decreases by a positive rise in N as seen in **Fig. 5. b.**

Table 5. The Skin friction factor, $C_{f\bar{x}}$, local Nusselt number, $Nu_{\bar{x}}$ and local Sherwood number, $Sh_{\bar{x}}$ for different values of the Biot number, Bi, with $\mathrm{Pr}=0.72$, $M=0.2$, $Sc=0.2$, $Ri=1$, $a=1$, $R=1$ and $N=1$.

Bi	$\mathrm{Re}_{\bar{x}}^{1/2}\,C_{f\bar{x}}$	$\mathrm{Re}_{\bar{x}}^{-1/2}\,Nu_{\bar{x}}$	$\mathrm{Re}_{\bar{x}}^{-1/2}\,Sh_{\bar{x}}$
0.1	0.038440	0.079168	0.264176
0.2	0.069660	0.131835	0.268651
0.3	0.091037	0.169820	0.271656
0.4	0.106703	0.198650	0.273830
0.5	0.118721	0.221334	0.275482
0.6	0.128250	0.239673	0.276782
0.7	0.136001	0.254820	0.277833
0.8	0.142435	0.267549	0.278702
0.9	0.147865	0.278401	0.279432
1.0	0.152510	0.287765	0.280055

doi:10.1371/journal.pone.0109404.t005

Table 6. The Skin friction factor, $C_{f\bar{x}}$, local Nusselt number, $Nu_{\bar{x}}$ and local Sherwood number, $Sh_{\bar{x}}$ for different values of the Schmidt number, Sc, with $\mathrm{Pr}=0.72,\ M=0.2,\ a=1,\ Ri=1,\ Bi=0.5,\ R=1$ and $N=1$.

Sc	$\mathrm{Re}_{\bar{x}}^{1/2}\,C_{f\bar{x}}$	$\mathrm{Re}_{\bar{x}}^{-1/2}\,Nu_{\bar{x}}$	$\mathrm{Re}_{\bar{x}}^{-1/2}\,Sh_{\bar{x}}$
0.22	0.114704	0.220421	0.289944
0.30	0.101054	0.217298	0.342816
0.60	0.068403	0.210346	0.498874
0.66	0.063793	0.209485	0.525015
0.78	0.055692	0.208058	0.573872

doi:10.1371/journal.pone.0109404.t006

- **Fig. 5. c** shows the response of the dimensionless concentration function through the boundary-layer regime to Prandtl number Pr.
- The dimensionless concentration function $\phi(\eta)$ as shown in **Fig. 5. d** is adversely affected through increasing the mixed convective parameter Ri. According to **Figs. 4. d.** and **5. d.** both temperature and concentration profiles descend smoothly from the maximum value at the wall to zero in the free stream. Here the value of the buoyancy ratio parameter is unity, $N=1$ which indicates that the thermal and concentration (species diffusion) buoyancy forces are of the same order of magnitude.
- **Fig. 5. e.** indicates that concentration $\phi(\eta)$ is reduced continuously throughout the boundary-layer with increasing the value of Sc. Schmidt number measures the relative effectiveness of momentum and mass transport by diffusion. Larger values of Sc are equivalent to reducing the chemical molecular diffusivity i.e. less diffusion therefore takes place by mass transport.
- **Fig 5. f.** shows that changing the value of the slip parameter a has little influence on the concentration profiles.

Conclusions

In this study, combined heat and mass transfer of the flow along a moving vertical flat plate with hydrodynamic slip and thermal convective boundary condition was considered. In order to reduce the two independent variables into one and hence to reduce the governing equations into a system of nonlinear ordinary differential equations, a linear group of transformations was used. The obtained equations were solved analytically using the differential transform method. The results were verified by results taken from the numerical method and excellent agreement was observed. The effects of different parameters on the skin friction factor, $C_{f\bar{x}}$, local Nusselt number, $Nu_{\bar{x}}$, and local Sherwood number $Sh_{\bar{x}}$ were shown and explained through tables and also changes of dimensionless flow and heat and mass transfer rates due to changes in some parameters were analyzed and presented graphically.

APPENDIX A

The governing boundary-layer equations in dimensional form are:

$$\frac{\partial \bar{u}}{\partial \bar{x}}+\frac{\partial \bar{v}}{\partial \bar{y}}=0, \tag{a1}$$

$$\rho\left(\bar{u}\frac{\partial \bar{u}}{\partial \bar{x}}+\bar{v}\frac{\partial \bar{u}}{\partial \bar{y}}\right)= \mu\frac{\partial^2 \bar{u}}{\partial \bar{y}^2}+[\rho g\beta_T\ (T-T_\infty)+\rho g\beta_C\,(C-C_\infty)]-\frac{\sigma_0 B_0^2}{\bar{x}}\,\bar{u}^2, \tag{a2}$$

$$\bar{u}\frac{\partial T}{\partial \bar{x}}+\bar{v}\frac{\partial T}{\partial \bar{y}}=\left(\alpha+\frac{16\ \sigma_1 T_\infty^3}{3\,\rho\,c_p\,k_1}\right)\frac{\partial^2 T}{\partial \bar{y}^2}, \tag{a3}$$

$$\bar{u}\frac{\partial C}{\partial \bar{x}}+\bar{v}\frac{\partial C}{\partial \bar{y}}=D\frac{\partial^2 C}{\partial \bar{y}^2}, \tag{a4}$$

subject to the boundary conditions:

$$\begin{aligned}&\bar{v}=0,\bar{u}=U_w+U_{\mathrm{slip}}=U_0\left(\frac{x}{L}\right)^{1/2}+N_1\upsilon\,\frac{\partial\,\bar{u}}{\partial\,\bar{y}},-k\,\frac{\partial\,T}{\partial\,\bar{y}}\\&=h_f(\bar{x})\left[T_f-T_w\right],\ C=C_w\ \text{ at }\ \bar{y}=0,\\&\bar{u}\to 0,\quad T\to T_\infty,\quad C\to C_\infty\quad\text{as}\quad \bar{y}\to\infty.\end{aligned} \tag{a5}$$

Using the following boundary-layer variables:

$$\begin{aligned}&x=\frac{\bar{x}}{L},y=\frac{\bar{y}\,\mathrm{Re}^{1/2}}{L},u=\frac{\bar{u}}{U_0},\\&v=\frac{\bar{v}\,L}{\upsilon\,\mathrm{Re}^{1/2}},\ \theta=\frac{T-T_\infty}{T_f-T_\infty},\ \phi=\frac{C-C_\infty}{C_w-C_\infty},\end{aligned} \tag{a6}$$

the following equations are obtained for Eqs. (a2)–(a4):

$$\begin{aligned}&\rho\left(uU_0\frac{\partial(uU_0)}{\partial(xL)}+\frac{\upsilon\mathrm{Re}^{1/2}}{L}v\frac{\partial(uU_0)}{\partial\left(\frac{yL}{\mathrm{Re}^{1/2}}\right)}\right)=\\&\mu\frac{\partial}{\partial\left(\frac{yL}{\mathrm{Re}^{1/2}}\right)}\left(\frac{\partial(uU_0)}{\partial\left(\frac{yL}{\mathrm{Re}^{1/2}}\right)}\right)+\rho g\beta_T\frac{T_f-T_\infty}{T-T_\infty}(T-T_\infty)\theta+\\&\rho g\beta_C\frac{C_w-C_\infty}{C-C_\infty}(C-C_\infty)\phi-\sigma_0 B_0^2\frac{(uU_0)^2}{xL},\end{aligned} \tag{a7}$$

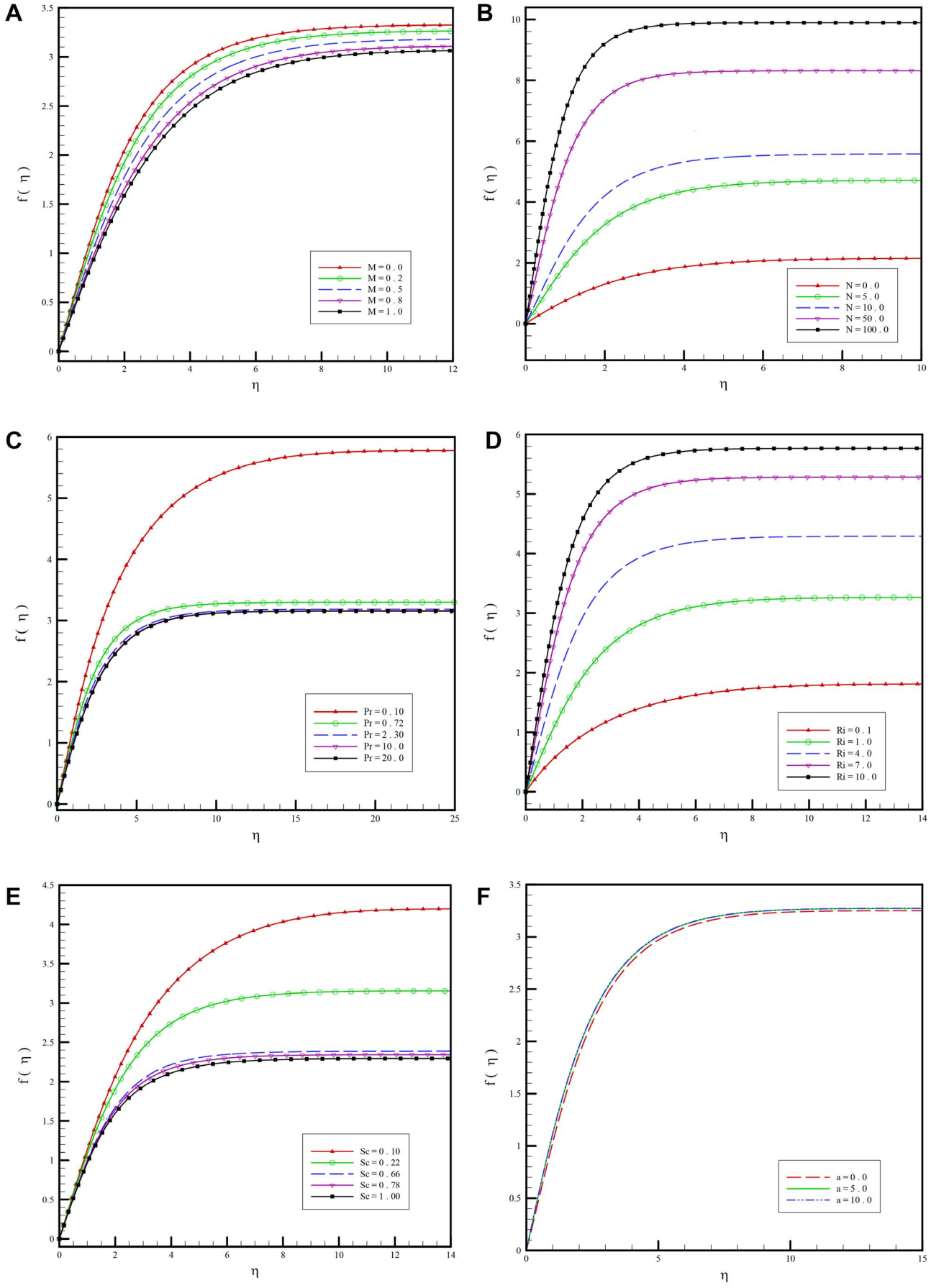
A
f(η)
η
M = 0 . 0
M = 0 . 2
M = 0 . 5
M = 0 . 8
M = 1 . 0
B
f(η)
η
N = 0 . 0
N = 5 . 0
N = 10 . 0
N = 50 . 0
N = 100 . 0
C
f(η)
η
Pr = 0 . 10
Pr = 0 . 72
Pr = 2 . 30
Pr = 10 . 0
Pr = 20 . 0
D
f(η)
η
Ri = 0 . 1
Ri = 1 . 0
Ri = 4 . 0
Ri = 7 . 0
Ri = 10 . 0
E
f(η)
η
Sc = 0 . 10
Sc = 0 . 22
Sc = 0 . 66
Sc = 0 . 78
Sc = 1 . 00
F
f(η)
η
a = 0 . 0
a = 5 . 0
a = 10 . 0

Figure 3. a. Variation of the dimensionless stream function for various values of magnetic field parameter M versus η when $a=1$, $\mathbf{Pr=0.72}$, $\boldsymbol{Sc=0.2}$, $\boldsymbol{Ri=1}$ and $N=1$. b. Variation of the dimensionless stream function for various values of buoyancy ration parameter N versus η when $a=1$, $\mathrm{Pr}=0.72$, $Ri=1$, $M=0.2$ and $Sc=0.2$. c. Variation of the dimensionless stream function for various values of Prandtl number Pr versus η when $a=1$, $M=0.2$, $Sc=0.2$, $Ri=1$ and $N=1$. d. Variation of the dimensionless stream function for various values of mixed convective parameter Ri versus η when $a=1$, $\mathrm{Pr}=0.72$, $Sc=0.2$, $M=0.2$ and $N=1$. e. Variation of the dimensionless stream function for various values of Schmidt number Sc versus η when $a=1$, $\mathrm{Pr}=0.72$, $Ri=1$, $M=0.2$ and $N=1$. f. Variation of the dimensionless stream function for various values of first order slip parameters a versus η when $\mathrm{Pr}=0.72$, $M=0.2$, $Sc=0.2$, $Ri=1$ and $N=1$.
doi:10.1371/journal.pone.0109404.g003

$$uU_0\frac{\partial\left(\left(T_f-T_\infty\right)\theta+T_\infty\right)}{\partial(xL)}+v\frac{\upsilon\mathrm{Re}^{1/2}}{L}\frac{\partial\left(\left(T_f-T_\infty\right)\theta+T_\infty\right)}{\partial\left(\frac{yL}{\mathrm{Re}^{1/2}}\right)}$$
$$=\left(\alpha+\frac{16\,\sigma_1T_\infty^3}{3\,\rho\,c_p\,k_1}\right)\frac{\partial}{\partial\left(\frac{yL}{\mathrm{Re}^{1/2}}\right)}\left(\frac{\partial\left(\left(T_f-T_\infty\right)\theta+T_\infty\right)}{\partial\left(\frac{yL}{\mathrm{Re}^{1/2}}\right)}\right), \tag{a8}$$

$$uU_0\frac{\partial((C_w-C_\infty)\phi+C_\infty)}{\partial(xL)}+v\frac{\upsilon\mathrm{Re}^{1/2}}{L}\frac{\partial((C_w-C_\infty)\phi+C_\infty)}{\partial\left(\frac{yL}{\mathrm{Re}^{1/2}}\right)}$$
$$=D\frac{\partial}{\partial\left(\frac{yL}{\mathrm{Re}^{1/2}}\right)}\left(\frac{\partial((C_w-C_\infty)\phi+C_\infty)}{\partial\left(\frac{yL}{\mathrm{Re}^{1/2}}\right)}\right). \tag{a9}$$

After simplifying the equations and dividing Eq. (a7) by $\rho\,U_0^2/L$, Eq. (a8) by $U_0\,\alpha\left(T_f-T_\infty\right)/L\,\upsilon$, Eq. (a9) by $U_0(C_w-C_\infty)/L$, and using the definitions for $\mathrm{Re}=U_0\,L/\upsilon$, $Ri=Gr/\mathrm{Re}^2$, $Gr=g\beta_T\left(T_f-T_\infty\right)L^3/\upsilon^2$, $N=\beta_C(C_w-C_\infty)/\beta_T(T_f-T_\infty)$, $M=\sigma_0\,B_0^2/\rho$, $R=16\,\sigma_1\,T_\infty^3/3\,k_1k$, $\mathrm{Pr}=\upsilon/\alpha$, and $Sc=\upsilon/D$ following equations are obtained:

$$u\frac{\partial u}{\partial x}+v\frac{\partial u}{\partial y}-\frac{\partial^2u}{\partial y^2}-Ri[\theta+N\phi]+\frac{M}{x}u^2=0, \tag{a10}$$

$$\mathrm{Pr}\left(u\frac{\partial T}{\partial x}+v\frac{\partial T}{\partial y}\right)-(1+R)\frac{\partial^2\theta}{\partial y^2}=0, \tag{a11}$$

$$Sc\left(u\frac{\partial C}{\partial x}+v\frac{\partial C}{\partial y}\right)-\frac{\partial^2\phi}{\partial y^2}=0. \tag{a12}$$

The stream function ψ defined as $u=\partial\psi/\partial y$, $v=-\partial\psi/\partial x$ is substituted into Eqs. (a10)–(a12) to reduce the number of equations and number of dependent variables, therefore the following three dimensionless equations are obtained:

$$\frac{\partial\psi}{\partial y}\frac{\partial^2\psi}{\partial x\,\partial y}-\frac{\partial\psi}{\partial x}\frac{\partial^2\psi}{\partial y^2}-\frac{\partial^3\psi}{\partial y^3}-Ri\,[\theta+N\,\phi]+\frac{M}{x}\left(\frac{\partial\psi}{\partial y}\right)^2=0, \tag{a13}$$

$$\mathrm{Pr}\left(\frac{\partial\psi}{\partial y}\frac{\partial\theta}{\partial x}-\frac{\partial\psi}{\partial x}\frac{\partial\theta}{\partial y}\right)-(1+R)\frac{\partial^2\theta}{\partial y^2}=0, \tag{a14}$$

$$Sc\left(\frac{\partial\psi}{\partial y}\frac{\partial\phi}{\partial x}-\frac{\partial\psi}{\partial x}\frac{\partial\phi}{\partial y}\right)-\frac{\partial^2\phi}{\partial y^2}=0. \tag{a15}$$

The boundary conditions take the following form:

$$\frac{\partial\psi}{\partial y}=x^{1/2}+\frac{\mathrm{Re}^{1/2}N_1(x)\,\upsilon}{L}\frac{\partial^2\psi}{\partial y^2},\ \frac{\partial\psi}{\partial x}=0,\ \frac{\partial\theta}{\partial y}=$$
$$-\frac{L\,h_f(x)}{k\,\mathrm{Re}^{1/2}}(1-\theta),\ \ \phi=1\ \text{at}\ \ y=0\,, \tag{a16}$$
$$\frac{\partial\psi}{\partial y}\to0,\ \ \theta\to0,\ \ \phi\to0\quad\text{as}\quad y\to\infty.$$

All independent and dependent variables are scaled as:

$$x^*=x\,A^{\alpha_1},\ y^*=y\,A^{\alpha_2},\ \psi^*=\psi\,A^{\alpha_3},$$
$$\theta^*=\theta\,A^{\alpha_4},\phi^*=\phi\,A^{\alpha_5}\,,h_f{}^*=h_f\,A^{\alpha_6},N_1{}^*=N_1\,A^{\alpha_7}, \tag{a17}$$

where $A,\alpha_i\,(i=1,2,...,6,7)$ are constants. The values of α_i should be chosen such that the form of the Eqs. (a13)–(a15) is invariant under the transformations by substituting the above variables:

$$\frac{A^{\alpha_1+2\alpha_2}}{A^{2\alpha_3}}\frac{\partial\psi^*}{\partial y^*}\frac{\partial^2\psi^*}{\partial x^*\partial y^*}-\frac{A^{\alpha_1+2\alpha_2}}{A^{2\alpha_3}}\frac{\partial\psi^*}{\partial x^*}\frac{\partial^2\psi^*}{\partial y^{*2}}$$
$$-\frac{A^{3\alpha_2}}{A^{\alpha_3}}\frac{\partial^3\psi^*}{\partial y^{*3}}-Ri\left[\frac{\theta^*}{A^{\alpha_4}}+\frac{N\phi^*}{A^{\alpha_5}}\right]+\frac{A^{\alpha_1+2\alpha_2}}{A^{2\alpha_3}}\frac{1}{x^*}\left(\frac{\partial\psi^*}{\partial y^*}\right)^2=0, \tag{a18}$$

$$\frac{A^{\alpha_1+\alpha_2}}{A^{\alpha_3+\alpha_4}}\frac{\partial\psi^*}{\partial y^*}\frac{\partial\theta^*}{\partial x^*}-\frac{A^{\alpha_1+\alpha_2}}{A^{\alpha_3+\alpha_4}}\frac{\partial\psi^*}{\partial x^*}\frac{\partial\theta^*}{\partial y^*}-\frac{A^{2\alpha_2}}{A^{\alpha_4}}(1+R)\frac{\partial^2\theta}{\partial y^2}=0, \tag{a19}$$

$$Sc\left(\frac{A^{\alpha_1+\alpha_2}}{A^{\alpha_3+\alpha_5}}\frac{\partial\psi^*}{\partial y^*}\frac{\partial\phi^*}{\partial x^*}-\frac{A^{\alpha_1+\alpha_2}}{A^{\alpha_3+\alpha_5}}\frac{\partial\psi^*}{\partial x^*}\frac{\partial\phi^*}{\partial y^*}\right)-\frac{A^{2\alpha_2}}{A^{\alpha_5}}\frac{\partial^2\phi^*}{\partial y^{*2}}=0. \tag{a20}$$

Boundary conditions:

$$\frac{\mathrm{A}^{\alpha_2}}{\mathrm{A}^{\alpha_3}}\frac{\partial\,\psi^*}{\partial y^*}=\mathrm{x}^{1/2}+\frac{\mathrm{A}^{2\alpha_2}}{\mathrm{A}^{\alpha_3+\alpha_7}}\frac{\mathrm{Re}^{1/2}\mathrm{N}^*{}_1(\mathrm{x})\,\upsilon}{\mathrm{L}}\frac{\partial^2\,\psi^*}{\partial y^{*2}},\quad\frac{\partial\psi^*}{\partial x^*}=0,$$
$$\frac{\mathrm{A}^{\alpha_2}}{\mathrm{A}^{\alpha_4}}\frac{\partial\theta^*}{\partial y^*}=-\frac{\mathrm{L\,h_f}^*(\mathrm{x})}{\mathrm{A}^{\alpha_6}\mathrm{k\,Re}^{1/2}}+\frac{\mathrm{L\,h_f}^*(\mathrm{x})}{\mathrm{A}^{\alpha_6+\alpha_4}\mathrm{k\,Re}^{1/2}}\theta^*,\phi^*=1\ \text{at}\ \mathrm{y}=0\,, \tag{a21}$$
$$\frac{\partial\,\psi^*}{\partial y^*}\to0,\ \theta^*\to0,\ \phi^*\to0\quad\text{as}\quad\mathrm{y}\to\infty.$$

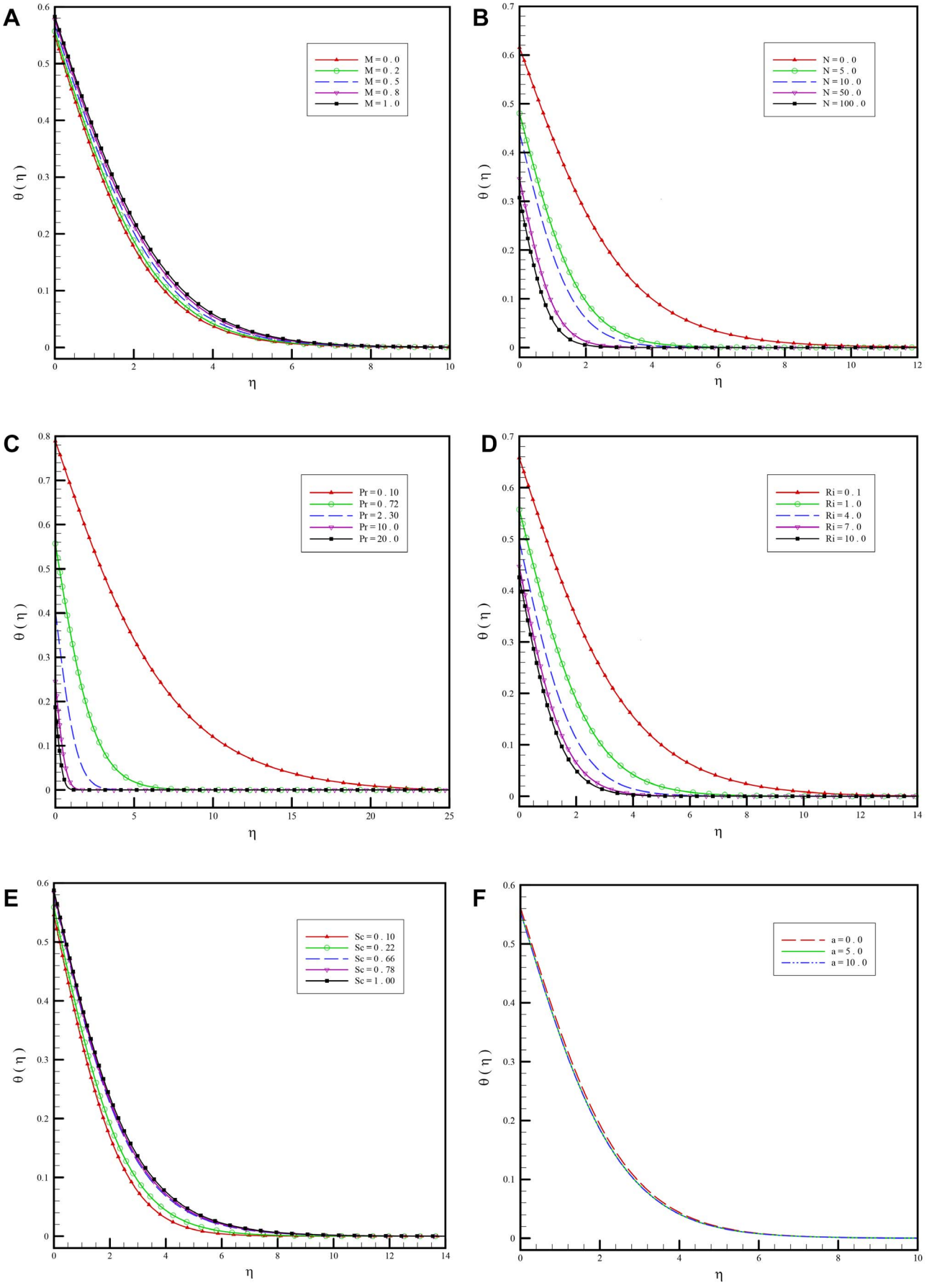
A
M = 0 . 0
M = 0 . 2
M = 0 . 5
M = 0 . 8
M = 1 . 0
θ (η)
η
B
N = 0 . 0
N = 5 . 0
N = 10 . 0
N = 50 . 0
N = 100 . 0
θ (η)
η
C
Pr = 0 . 10
Pr = 0 . 72
Pr = 2 . 30
Pr = 10 . 0
Pr = 20 . 0
θ (η)
η
D
Ri = 0 . 1
Ri = 1 . 0
Ri = 4 . 0
Ri = 7 . 0
Ri = 10 . 0
θ (η)
η
E
Sc = 0 . 10
Sc = 0 . 22
Sc = 0 . 66
Sc = 0 . 78
Sc = 1 . 00
θ (η)
η
F
a = 0 . 0
a = 5 . 0
a = 10 . 0
θ (η)
η

Figure 4. a. Variation of the dimensionless temperature for various values of magnetic field parameter M versus η when $a=1$, $\mathbf{Pr}=0.72$, $Sc=0.2$, $Ri=1$ and $N=1$. b. Variation of the dimensionless temperature for various values of buoyancy ration parameter N versus η when $a=1$, $\mathrm{Pr}=0.72$, $Ri=1$, $M=0.2$ and $Sc=0.2$. c. Variation of the dimensionless temperature for various values of PrandtI numberPr versus η when $a=1$, $M=0.2$, $Sc=0.2$, $Ri=1$ and $N=1$. d. Variation of dimensionless temperature for various values of mixed convective parameter Ri versus η when $a=1$, $\mathrm{Pr}=0.72$, $Sc=0.2$, $M=0.2$ and $N=1$. e.-Variation of the dimensionless temperature for various values of Schmidt number Sc versus η when $a=1$, $\mathrm{Pr}=0.72$, $Ri=1$, $M=0.2$ and $N=1$. f. Variation of the dimensionless temperature for various values of first order slip parameters a versus η when $\mathrm{Pr}=0.72$, $M=0.2$, $Sc=0.2$, $Ri=1$ and $N=1$.
doi:10.1371/journal.pone.0109404.g004

Obviously Eqs. (a18)–(a20) will be invariant if α_i are related by

$$\alpha_1=4\alpha_2,\ \alpha_3=3\alpha_2,\ \alpha_4\ =\ \alpha_5=0,\alpha_6=-\alpha_2,\ \alpha_7=\alpha_2. \tag{a22}$$

Using the similarity independent variable $\eta=\frac{y}{\sqrt[4]{x}}$ and other absolute invariants such as dimensionless velocity, temperature, concentration function as follows:

$$\begin{aligned}&\psi=\ x^{3/4}f(\eta),\theta=\theta(\eta),\\&\phi=\phi(\eta),\ h_f=x^{-1/4}(h_f)_0,N_1=x^{1/4}(N_1)_0,\end{aligned} \tag{a23}$$

the following equations are obtained:

$$\begin{aligned}&\left(x^{2/4}f'(\eta)\right)\left(\frac{1}{2}x^{-2/4}f'(\eta)-\frac{y}{4}x^{-3/4}f''(\eta)\right)-\\&\left(\frac{3}{4}x^{-1/4}f(\eta)-\frac{y}{4}x^{-2/4}f'(\eta)\right)\left(x^{1/4}f''(\eta)\right)\\&-f'''(\eta)-Ri[\theta+N\phi]+\frac{M}{x}\left(x^{2/4}f'(\eta)\right)^2=0,\end{aligned} \tag{a24}$$

$$\begin{aligned}&\mathrm{Pr}\left[\begin{array}{l}\left(x^{2/4}f'(\eta)\right)\left(-\frac{y}{4}x^{-5/4}\theta'(\eta)\right)\\-\left(\frac{3}{4}x^{-1/4}f(\eta)-\frac{y}{4}x^{-2/4}f'(\eta)\right)\left(x^{-1/4}\theta'(\eta)\right)\end{array}\right]-\\&(1+R)\left(x^{-2/4}\theta''(\eta)\right)=0,\end{aligned} \tag{a25}$$

$$\begin{aligned}&Sc\left[\begin{array}{l}\left(x^{2/4}f'(\eta)\right)\left(-\frac{y}{4}x^{-5/4}\phi'(\eta)\right)\\-\left(\frac{3}{4}x^{-1/4}f(\eta)-\frac{y}{4}x^{-2/4}f'(\eta)\right)\left(x^{-1/4}\phi'(\eta)\right)\end{array}\right]-\\&x^{-2/4}\phi''(\eta)=0.\end{aligned} \tag{a26}$$

After simplifying the above equations, Eqs. (16)–(18) are obtained.

APPENDIX B

Suppose that a power series $\sum_{i=0}^{\infty}a_ix^i$ is given, which represents a function $f(x)$, such that:

$$f(x)=\sum_{i=0}^{\infty}a_ix^i. \tag{b1}$$

The Páde approximant is a rational fraction and the notation for such a Padé approximant is:

$$[L/M]=\frac{P_L(x)}{Q_M(x)}, \tag{b2}$$

where $P_L(x)$ is a polynomial of degree at most L and $Q_M(x)$ is a polynomial of degree at most M. Therefore:

$$f(x)=a_0+a_1x+a_2x^2+a_3x^3+a_4x^4+\cdots, \tag{b3}$$

$$P_L(x)=p_0+p_1x+p_2x^2+p_3x^3+\ldots+p_Lx^L, \tag{b4}$$

$$Q_M(x)=q_0+q_1x+q_2x^2+q_3x^3+\ldots+q_Mx^M, \tag{b5}$$

where in Eq. (b2) there are $L+1$ numerator coefficients and $M+1$ denominator coefficients. Since the numerator and denominator can be multiplied by a constant and $[L/M]$ left unchanged, the following normalization condition is imposed

$$Q_M(0)=1. \tag{b6}$$

So there are $L+1$ independent numerator coefficients and M independent denominator coefficients, which make $L+M+1$ unknown coefficients in all. This number suggests that normally the $[L/M]$ ought to fit the power series Eq. (b1) through the orders $1,x,x^2,\ldots,x^{L+M}$. Based on conditions given in [44,45], $[L/M]$ approximation is uniquely determined. In the notation of formal power series:

$$\begin{aligned}&\sum_{i=0}^{\infty}a_ix^i=\\&\frac{p_0+p_1x+p_2x^2+p_3x^3+\ldots+p_Lx^L}{q_0+q_1x+q_2x^2+q_3x^3+\ldots+q_Mx^M}+O\left(x^{L+M+1}\right).\end{aligned} \tag{b7}$$

By cross-multiplying Eq. (b7), one obtains:

$$\begin{aligned}&\left(q_0+q_1x+q_2x^2+q_3x^3+\ldots+q_Mx^M\right)\\&\times\left(a_0+a_1x+a_2x^2+a_3x^3+a_4x^4+\ldots\right)\\&=p_0+p_1x+p_2x^2+p_3x^3+\ldots+p_Lx^L+O\left(x^{L+M+1}\right).\end{aligned} \tag{b8}$$

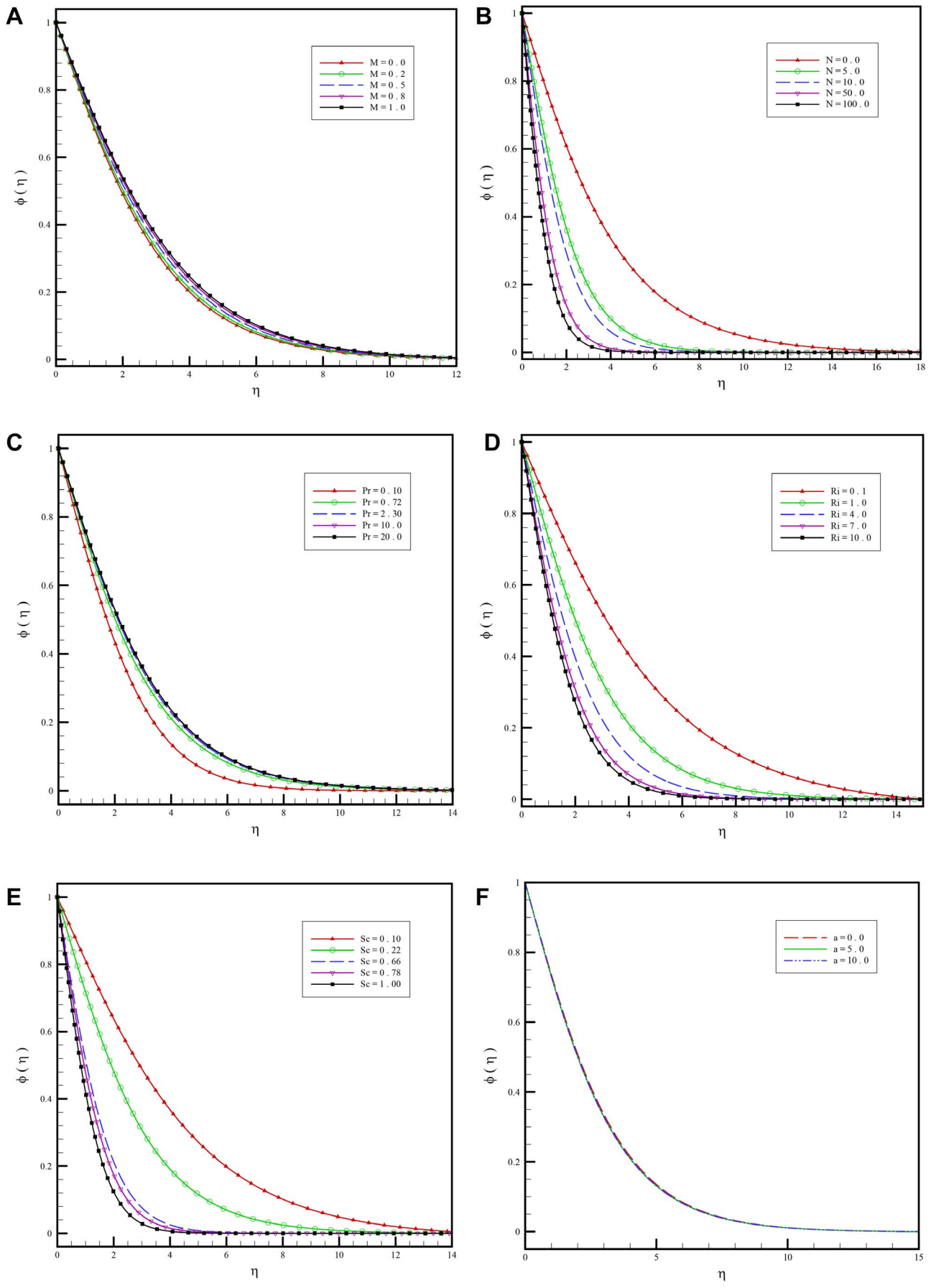
A
M = 0 . 0
M = 0 . 2
M = 0 . 5
M = 0 . 8
M = 1 . 0
ϕ (η)
η
B
N = 0 . 0
N = 5 . 0
N = 10 . 0
N = 50 . 0
N = 100 . 0
ϕ (η)
η
C
Pr = 0 . 10
Pr = 0 . 72
Pr = 2 . 30
Pr = 10 . 0
Pr = 20 . 0
ϕ (η)
η
D
Ri = 0 . 1
Ri = 1 . 0
Ri = 4 . 0
Ri = 7 . 0
Ri = 10 . 0
ϕ (η)
η
E
Sc = 0 . 10
Sc = 0 . 22
Sc = 0 . 66
Sc = 0 . 78
Sc = 1 . 00
ϕ (η)
η
F
a = 0 . 0
a = 5 . 0
a = 10 . 0
ϕ (η)
η

Figure 5. a. Variation of the dimensionless concentration function for various values of magnetic field parameter M versus η when $a=1$, $\mathbf{Pr}=0.72$, $Sc=0.2$, $Ri=1$ and $N=1$. b. Variation of the dimensionless concentration function for various values of buoyancy ration parameter N versus η when $a=1$, $\mathrm{Pr}=0.72$, $Ri=1$, $M=0.2$ and $Sc=0.2$. c. Variation of the dimensionless concentration function for various values of Prandtl number Pr versus η when $a=1$, $M=0.2$, $Sc=0.2$, $Ri=1$ and $N=1$. d. Variation of the dimensionless concentration function for various values of mixed convective parameter Ri versus η when $a=1$, $\mathrm{Pr}=0.72$, $Sc=0.2$, $M=0.2$ and $N=1$. e. Variation of the dimensionless concentration function for various values of Schmidt number Sc versus η when $a=1$, $\mathrm{Pr}=0.72$, $Ri=1$, $M=0.2$ and $N=1$. f. Variation of the dimensionless concentration function for various values of first order slip parameters a versus η when $\mathrm{Pr}=0.72$, $M=0.2$, $Sc=0.2$, $Ri=1$ and $N=1$.
doi:10.1371/journal.pone.0109404.g005

From Eq. (b8) the following set of linear equations is obtained

$$\begin{cases} a_0 = p_0, \\ a_1 + a_0 q_1 = p_1, \\ a_2 + a_1 q_1 + a_0 q_2 = p_2, \\ \vdots \\ a_L + a_{L-1} q_1 + \cdots + a_0 q_L = p_L, \end{cases} \tag{b9}$$

and

$$\begin{cases} a_{L+1} + a_L q_1 + \cdots + a_{L-M+1} q_M = 0, \\ a_{L+2} + a_{L+1} q_1 + \cdots + a_{L-M+2} q_M = 0, \\ \vdots \\ a_{L+M} + a_{L+M-1} q_1 + \cdots + a_L q_M = 0, \end{cases} \tag{b10}$$

where $a_n = 0$ for $n<0$ and $q_j = 0$ for $j>M$. Equations (b9) and (b10) can be solved directly provided they are non-singular.

$$[L/M] = \frac{\begin{vmatrix} a_{L-m+1} & a_{L-M+2} & \cdots & a_{L+1} \\ \vdots & \vdots & \ddots & \vdots \\ a_L & a_{L+1} & \cdots & a_{L+M} \\ \sum_{j=M}^{L} a_{j-M} x^j & \sum_{j=M-1}^{L} a_{j-M+1} x^j & \cdots & \sum_{j=0}^{L} a_j x^j \end{vmatrix}}{\begin{vmatrix} a_{L-M+1} & a_{L-M+2} & \cdots & a_{L+1} \\ \vdots & \vdots & \ddots & \vdots \\ a_L & a_{L+1} & \cdots & a_{L+M} \\ x^M & x^{M-1} & \cdots & 1 \end{vmatrix}}. \tag{b11}$$

If the lower index on a sum exceeds the upper, the sum is replaced by zero. Alternate forms are:

$$\begin{aligned} [L/M] &= \sum_{j=0}^{L-M} a_j x^j + x^{L-M+1} w_{L/M}^T W_{L/M}^{-1} w_{L/M} \\ &= \sum_{j=0}^{L+n} a_j x^j + x^{L+n+1} w_{(L+M)/M}^T W_{L/M}^{-1} w_{(L+n)/M}, \end{aligned} \tag{b12}$$

for

$$W_{L/M} = \begin{bmatrix} a_{L-M+1} - x a_{L-M+2} & \cdots & a_L - x a_{L+1} \\ \vdots & \ddots & \vdots \\ a_L - x a_{L+1} & \cdots & a_{L+M+1} - x a_{L+M} \end{bmatrix}, \tag{b13}$$

$$w_{L/M} = \begin{bmatrix} a_{L-M+1} \\ a_{L-M+2} \\ \vdots \\ a_L \end{bmatrix}. \tag{b14}$$

The construction of $[L/M]$ approximants involves only algebraic operations [44,45]. Each choice of L, degree of the numerator and M, degree of the denominator, leads to an approximant. How to direct the choice in order to obtain the best approximant is the major difficulty in applying the technique, which necessitates the need for a criterion for the choice depending on the *shape* of the solution. A criterion which has worked well here is the choice of $[L/M]$ approximants such that $L=M$. The approximants are constructed using **MATHEMATICA** software.

Acknowledgments

The authors express their gratitude to the anonymous referees for their constructive reviews of the manuscript and for helpful comments which have improved the paper.

SA acknowledges support from the NRF, Pretoria, South Africa.

Author Contributions

Analyzed the data: NK SA MJU NF. Wrote the paper: MMR NK SA MJU NF. Performed computation: NK SA MJU NF. Agree with manuscript results and conclusions: MMR NK SA MJU NF. Interaction with PLOS: SA.

References

1. Lyapunov AM (1992) The General Problem of the Stability of Motion Taylor & Francis London UK English translation.
2. Karmishin AV, Zhukov AI, Kolosov VG (1990) Methods of Dynamics Calculation and Testing for Thin-Walled Structures Mashinostroyenie Moscow Russia.
3. He JH (1999) Homotopy perturbation technique, Comp Meth Appl Mech Engin 178(3–4): 257–262.
4. Rashidi MM, Ganji DD (2010) Homotopy perturbation method for solving flow in the extrusion processes. Int J Eng 23(3–4): 267–272.
5. He JH (1997) A new approach to non-linear partial differential equations. Commun Nonlin Sci Numer Simul 2(4): 230–235.

6. Rashidi MM, Shahmohamadi H (2009) Analytical solution of three-dimensional Navier–Stokes equations for the flow near an infinite rotating disk. Commun Nonlin Sci Numer Simul 14(7): 2999–3006.
7. Liao S (2004) on the homotopy analysis method for nonlinear problems. Appl Math Comput 147: 499–513.
8. Bég OA, Rashidi MM, Kavyani N, Islam MN (2013) Entropy generation in magnetohydrodynamic convective Von Kármán swirling flow: Homotopy analysis. Int J Appl Math Mech 9(4): 37–65.
9. Zhou JK (1986) Differential Transformation and its Applications for Electrical Circuits Huazhong University Press Wuhan China.
10. Chen CK, Ho SH (1999) Solving partial differential equations by two dimensional differential transform method. Appl Math Comput 106: 171–179.
11. Ayaz F (2004) Solutions of the systems of differential equations by differential transform method. Appl Math Comput 147: 547–567.
12. Rashidi MM, Keimanesh M (2010) Using differential transform method and Padé approximant for solving MHD flow in a laminar liquid film from a horizontal stretching surface. Math Prob Engin 1–14.
13. Rashidi MM, Laraqi N, Sadri SM (2010) A novel analytical solution of mixed convection about an inclined flat plate embedded in a porous medium using the DTM-Padé. Int J Thermal Sci 49: 2405–2412.
14. Rashidi MM, Mohimanian Pour SM (2010) A novel analytical solution of heat transfer of a micropolar fluid through a porous medium with radiation by DTM-Padé. Heat Transfer-Asian Res 39, 575–589.
15. Chen CH (2004) Heat and mass transfer in MHD flow by natural convection from a permeable, inclined surface with variable wall temperature and concentration. Acta Mech 172: 219–235.
16. Damseh RA, Duwairi HM, Al-Odat M (2006) Similarity analysis of magnetic field and thermal radiation effects on forced convection flow. Turk J Eng Env Sci 30: 83–89.
17. Kaya A, Aydin O (2012) Effects of MHD and thermal radiation on forced convection flow about a permeable horizontal plate embedded in a porous medium Isı BilimiveTekniğiDergisi. J Thermal Sci Tech 32(1): 9–17.
18. Spreiter JR, Rizzi AW (1974) Aligned magnetohydrodynamic solution for solar wind flow past the earth's magnetosphere. Acta Astronaut 1(1–2): 15–35.
19. Nath O, Ojha SN, Takhar HS (1991) A study of stellar point explosion in a radiative magnetohydrodynamic medium. Astrophys Space Sci 183: 135–145.
20. Noor NFM, Abbasbandy S, Hashim I (2012) Heat and mass transfer of thermophoretic MHD flow over an inclined radiate isothermal permeable surface in the presence of heat source/sink. Int J Heat Mass Trans 55: 2122–2128.
21. Elbashbeshy EMA, Emam TG, Abdelgaber KM (2012) Effects of thermal radiation and magnetic field on unsteady mixed convection flow and heat transfer over an exponentially stretching surface with suction in the presence of internal heat generation/absorption. J Egypt Math Soc 20: 215–222.
22. Abd El-Aziz M (2013) Unsteady mixed convection heat transfer along a vertical stretching surface with variable viscosity and viscous dissipation. J Egypt Math Soc In press.
23. Sakiadis BC (1961) Boundary layer behaviour on continuous solid surface: I. Boundary-layer equations for two dimensional and axisymmetric flow. AIChE J 7 (1): 26–28.
24. Chien-Hsin C (2009) Magnetohydrodynamic mixed convection of a power-law fluid past a stretching surface in the presence of thermal radiation and internal heat generation/absorption. Int J Non-Linear Mech 44: 596–603.
25. Pal D, Chatterjee S (2011) Mixed convection magnetohydrodynamic heat and mass transfer past a stretching surface in a micropolar fluid-saturated porous medium under the influence of Ohmic heating, Soret and Dufour effects. Commun Nonlin Sci Numer Simul 16: 1329–1346.
26. Uddin MJ, Bég OA, Rashidi MM, Kavyani N (2014) Double-diffusive radiative magnetic mixed convective slip flow with Biot and Richardson number effects. J Eng Thermophys 23: 79–97.
27. Thompson PA, Troian SM (1997) A general boundary condition for liquid flow at solid surfaces. Nature 389: 360–362.
28. Nguyen NT, Wereley ST (2009) Fundamentals and Applications of Microfluidics Artech House, London 2nd Ed.
29. Karniadakis G, Beskok A, Aluru N (2005) Microflows and nanoflows fundamentals and simulation. In: Microflows and nanoflows fundamentals and simulation Springer Science New York.
30. Li D (2008) Encyclopedia of Microfluidics and Nanofluidics. Springer.
31. Kim BH, Beskok A, Cagin T (2010) Viscous heating in nanoscale shear driven liquid flows. Microfluid Nanofluid 9: 31–40.
32. Martin MJ, Boyd ID (2006) Momentum and heat transfer in laminar boundary layer with slip flow. J Thermophys Heat Trans (20): 710–719.
33. Kuznetsov AV, Nield DA (2010) Corrigendum to 'Forced convection with slip-flow in a channel occupied by a hyperporous medium saturated by a rarefied Gas'. Transp. Porous Media (2006) 64: 161–170 and 'Thermally developing forced convection in a porous medium occupied by a rarefied gas: parallel plate channel or circular tube with walls at constant heat flux' Transp. Porous Media (2009) 76: 345–362 Transp. Porous Media 85(2): 657–658.
34. Aziz A (2009) A similarity solution for laminar thermal boundary layer over flat plate with convective surface boundary condition. Commun Nonlin Sci Numer Simul 14: 1064–1068.
35. Magyari E (2011) Comment on "A similarity solution for laminar thermal boundary layer over a flat plate with a convective surface boundary condition" Aziz A (2009). Comm Nonlin Sci Numer Simul 14: 1064–1068 Commun Non. Sci. Num. Simul. 16: 599–601.
36. Ishak A (2010) Similarity solutions for flow and heat transfer over permeable surface with convective boundary conditions. Appl Math Comput 217(2): 837–842.
37. Rahman MM, Uddin MJ, Aziz A (2009) Effects of variable electric conductivity and non-uniform heat source (or sink) on convective micropolar fluid flow along an inclined flat plate with surface heat flux. Int J Therm Sci 48(12): 2331–2340.
38. Rohni AM, Ahmad S, Ismail AIM, Pop I (2013) Boundary layer flow and heat transfer over an exponentially shrinking vertical sheet with suction. Int J Therm Sci 4: 264–272.
39. Rashidi MM, Kavyani N, Bég OA, Gorla RSR (2013) Transient magnetohydrodynamic film flow, heat transfer and entropy generation from a spinning disk system: DTM-Padé semi-numerical simulation. Int J Energy Tech 5(18): 1–14.
40. Broyden CG (1965) A class of methods for solving non-linear simultaneous equations. Math Comput 19: 577–593.
41. Broyden CG (2000) On the discovery of the "good Broyden method". Math Prog Ser B 87: 209–213.
42. Keller HB (1992) Numerical methods for two-point boundary value problems Dover Publishing Inc. New York
43. Ascher UM, Mattheij RMM, Russell RD (1995) Numerical solution of boundary value problems for ordinary differential equations SIAM Philadelphia.
44. Baker GA, Graves-Morris P (1981) Encyclopedia of mathematics and its application 13, Parts I and II- Padé approximants, Addison-Wesley New York.
45. Baker GA (1975) Essentials of Padé Approximants. Academic Press London.